Development of a High Efficiency Solar Cell Using Adaptive Self-Cooling

Tiasha Joardar ©

5124 Water Haven Lane

Plano, TX 75093

Acknowledgements

First I would like to thank Mr. Neil Milburn for his help and guidance with the entire science fair process. I would like to thank my father for purchasing all the items required for this project, for his help with constructing some of the apparatus, for allowing me to use the garage and laundry room, for explaining several electrical and thermal concepts, and for proof reading and help with formatting this report. All experimental work was done in our home in Plano, Texas.

Abstract

In this project, a smart hybrid solar cell using self-powered adaptive temperature control is developed. Active temperature regulation is implemented using thermoelectric cooling modules and a synchronous switching circuit with variable duty cycle that periodically diverts the solar cell's output to a thermoelectric cooling module. A secondary watchdog circuit is implemented using an 8-bit microcontroller that periodically compares the cell temperature with the ambient air temperature and algorithmically adjusts the switching duty cycle to minimize the difference between the two temperatures. The performance of such a cell is compared to that of a conventional photovoltaic solar cell operating under identical environmental conditions. The basis of this comparison is the power output by each system. It is found that the hybrid self-cooled solar cell produces up to *10.25% more power* when compared to a conventional solar cell operating under identical conditions. This project is expected to lead to a cost-effective and environmentally friendly energy source.

Table of Contents

1. **Introduction** …… 7
   - 1.1 Problem Statement……..... 8
   - 1.2 Fundamentals of Photovoltaic Solar Cells ……..... 8
   - 1.3 Fundamentals of Solid State Thermoelectric Cooling ……....……. 11
   - 1.4 Self-Cooling Concept Used in This Project ……....…….…… 11
   - 1.5 Review of Prior Work…….……..... 13
2. **Theory**……..……12
   - 2.1 Single Stage Thermoelectric Cooling …….....14
   - 2.2 Design Innovations Based on Theoretical Analysis ……..…… 18
   - 2.3 Theoretical Calculations and Hypothesis …… ……19
3. **Experimental Setup and Procedures** …...…….. 20
   - 3.1 Variables……..…….. 20
   - 3.2 Apparatus Used…….…… 20
   - 3.3 Measurement Procedures…….....23
4. **Experimental Results**…… 23
   - 4.1 Power Output Loss in Solar Cell with Temperature ……..……... 23
   - 4.2 Power Recovery in Thermoelectric Cooled Hybrid Solar Cell …….……..... 25
   - 4.3 Optimum Thermoelectric Power Point for Maximum Solar Power…..…… 28
5. **Discussion**……...……29
6. **System Cost Comparisons**…….……31
7. **Future Work**……...33
8. **Conclusions**……33
9. **References** ……..34

List of Figures

Fig. 1 Simplified diagram of a TEC showing (a) a single junction and (b) an assembled view of a TEC module.. 9

Fig. 2 Theoretical dependence of optimum COP of a TEC module on its hot side temperature. 11

Fig. 3 Theoretically calculated plots of indoor temperature, cooling power, and COP as a function of current passed through a single-stage thermoelectric air conditioning system. 14

Fig. 4 Diagram showing a two-stage thermoelectric cooling system. 14

Fig. 5 Theoretically calculated variation of cold side temperature T_C with currents in the upper and lower TECs. (a) is a 3-d surface plot and (b) is a contour plot of the data. 16

Fig. 6 3-d surface plot of COP versus IC and IH for the two-stage system described in this section. 17

Fig. 7 Theoretically calculated T_C as a function of input power for T_H = 37°C and Q_{gen} = 4W. 18

Fig. 8 .Diagram showing how an active water cooled heat sink is used to control the temperature of the hot side of the TEC. 19

Fig. 9 Diagram showing equipment used to monitor energy usage by different air conditioning units. 21

Fig. 10 (a) Diagram of the single-stage, quad-module thermoelectric cooling system, (b) diagram of the two-stage cascaded thermoelectric system, and (c) photograph of fully assembled cascaded thermoelectric cooling unit used in this project. 22

Fig. 11 Energy consumed as a function of time by the vapor compression air conditioner over a 20 minute duration for three different ΔT settings, each with a heat load of 24W. 24

Fig. 12 Temperature inside home as a function of time for the vapor compression air conditioner for different ΔT values. 24

Fig. 13 Summary of energy used over one hour by the vapor compression system as a function of indoor temperature setting. 25

Fig. 14 Energy consumed as a function of time by the single-stage, single-module, thermoelectric air conditioner over a 20 minute duration for three different ΔT settings, each with a heat load of 24W. 26

Fig. 15 Temperature inside home as a function of time for the single-stage, single-module, thermoelectric air conditioner over a 20 minute duration for different ΔT settings. 26

Fig. 16 Measured variation of indoor temperature versus electrical energy used over one hour by a single-stage single-module thermoelectric system. 27

Fig. 17 Measured variation of indoor temperature (blue) and energy consumed in one hour versus electrical current input for a single-stage quad-module thermoelectric system. 28

Fig. 18 Measured variation of indoor temperature versus (a) electrical current IH, and (b) versus hourly energy use for a dual-stage cascaded thermoelectric system. 29

Fig. 19 Comparison of energy usage of vapor compression and thermoelectric air conditioning systems as a function of ΔT with a heat load of 24W. 30

Fig. 20 Dependence of purchase price of vapor compression air conditioners on cooling power found from a market survey (dots). Dashed line represents estimated dependence of cost per cooling watt for TEC systems based on current market prices. 31

1. Introduction

Although solar cells are currently one of the most reliable and effective sources of "green" energy, limits on their energy conversion efficiency are preventing them from becoming practical alternatives to fossil fuels in spite of several years of research and development. Efficiencies of photovoltaic solar cells have improved a lot in the past two decades [1 - 5]. But for solar technology to compete successfully against fossil fuels it is more important to drive down the cost per watt (CPW) of electricity generated. CPW is a direct function of the solar power system cost, and inversely related to the power output of the panels used. It is therefore important to keep the system cost low and increase cell power output. Over and above the intrinsic limits on efficiency of solar cells, in actual field use there is a further degradation in performance as solar cells heat up in sunlight, leading to additional loss of power. In this project a novel approach to recovering some of this lost power is investigated.

The basis of this effort lies in careful utilization of the thermoelectric effect. Thermoelectric cooling modules (TECs) pump heat from a high temperature region to a low temperature region by passing an electric current through a thermoelectric material. Since this does not require compressors or refrigerants, and since its cooling power can be electrically controlled, it may be possible to develop a suitable heat pump that limits the loss of solar cell power by keeping its temperature from rising above the ambient value.

In this project, a thermoelectrically self-cooled solar cell is developed. The system includes a microcontroller based temperature regulation mechanism which adaptively changes the cooling power used by the thermoelectric units depending on ambient conditions, thereby keeping cell temperature from rising above the outside air temperature. Since the practical use of such a system will depend entirely on how well it compares against a conventional solar cell, this aspect is the main theme of this project. The basis for comparison will be the energy output of each cell operating under identical environmental conditions.

It should be mentioned that the viability of thermoelectric cooling of solar cells depends critically on the cooling efficiency of the thermoelectric heat pump. The cooling efficiency of a thermoelectric heat pump is normally stated in terms of its Coefficient of Performance (COP) which is defined as the ratio of the amount of heat energy pumped by the system to the amount of electric energy required to do so. The higher the COP of a system, the lower its energy

consumption under constant heat loads. As will be detailed later, and contrary to common perceptions, the COP of thermoelectric heat pumps can actually be quite high when they are operated at low heat loads and low temperature differentials. Since these are the exact conditions under which normal solar panels operate, it is expected that thermoelectric based approach being pursued in this project will be effective.

1.1 Problem Statement

The main question addressed in this project can be stated quantitatively as follows.

> **Is it possible to develop and optimize a hybrid self-cooled solar cell using thermoelectric temperature control that produces at least *5% more net power* when compared to a conventional solar cell operating under identical conditions? A secondary question is whether the output energy cost per watt can be reduced by 5%.**

The choice of a 5% improvement target is loosely based on preliminary cost analysis of photovoltaic solar energy systems. It is estimated that a 5% increase in power output of a solar cell will reduce the cost per watt of electricity to a point where it starts becoming cost competitive with conventional sources of energy.

1.2 Fundamentals of Photovoltaic Solar Cells

Photovoltaic solar cells are basically p-n junction diodes. In this section relevant aspects of solar cell operation are discussed, in particular the change in electrical performance as a function of temperature.

The electrical behavior of a solar cell can be represented by the simplified equivalent circuit shown in Fig. 3. The relationship between the voltage V across an ideal solar cell and the current flowing through it is given as:

$$I = I_s(e^{V/Vt} - 1) - I_{SC} \tag{1}$$

where V_t is a constant (about 0.026V at 27°C) , I_s is the saturation current which depends mainly on how the solar cell is constructed, and I_{SC} is the short-circuit current generated by the photoelectric effect. Fig. 1. shows a simple equivalent circuit of a solar cell.

A related quantity of interest is the open-circuit voltage V_{oc}, which is the value of V when I equals to zero:

$$V_{OC} = V_t \ln\left(\frac{I_{SC}}{I_s}\right) \tag{2}$$

The power output of a solar cell can be determined from the product of I and V. Fig. 2 shows a typical I-V behavior and the related P-V behavior as obtained from equation (1). The main point is that there a specific (V_{mp}, I_{mp}) combination at which the power output is a maximum. Solar cells are normally operated at this peak power point. The peak power itself is given as:

$$P_{peak} = I_{SC} V_{OC} FF \tag{3}$$

where *FF* is called the "Fill Factor" which is a measure of the squareness of the I-V curve as depicted in Fig. 2

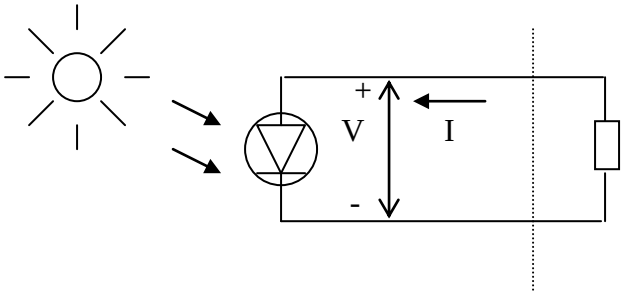

Fig. 1 Simple equivalent circuit of a photovoltaic solar cell.

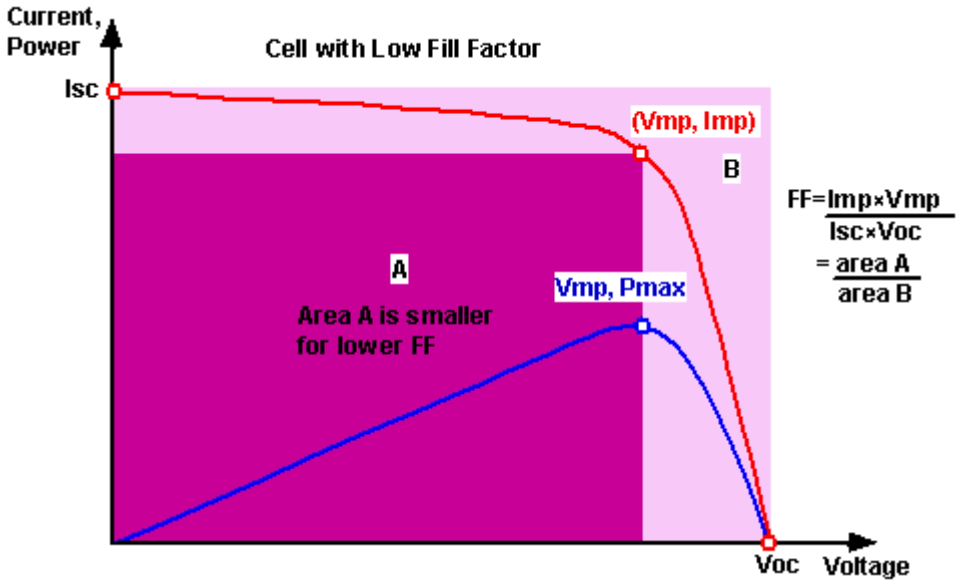

Fig. 2. Typical I-V (red) and P-V (blue) curves of a PV solar cell.

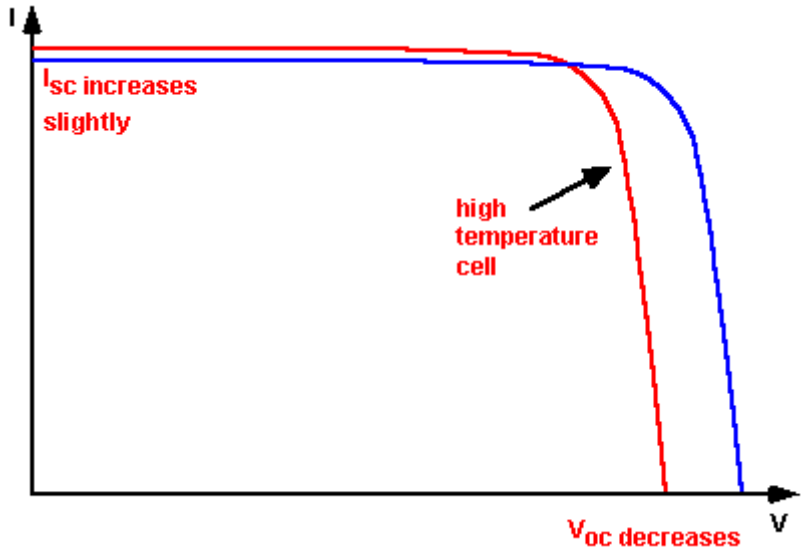

Fig. 3. Typical hot (red) and cold (blue) I-V curves of a PV solar cell.

Next, the temperature dependence of peak power is considered. Fig. 3 shows pictorially how the I-V behavior of a solar cell changes with temperature. The main points are that the short-circuit current I_{SC} and the fill-factor FF are very weak functions of temperature. On the other hand, the open-circuit voltage V_{OC} changes significantly with temperature. In typical Si solar cells V_{OC} drops about 2.2 mV per degree Celcius change in temperature. The total combined effect of temperature on the peak power output of a solar cell can be written as:

$$\frac{dP_{peak}}{dT} = -0.005 P_{peak} \tag{4}$$

where T represents the cell temperature. Equation (4) is an ordinary differential equation whose solution is given as:

$$P_{peak}(T_2) = P_{peak}(T_1) e^{-0.005(T2-T1)} \tag{5}$$

where T_2 and T_1 are two different temperatures. (5) implies that the peak power decreases exponentially with increase in temperature.

A lot of research is currently in progress on trying to improve the efficiency and power output of photovoltaic solar cells[6]. However, the intrinsic efficiency of PV cells is not the focus of this project and therefore discussion of this aspect will be kept to a minimum.

1.3 Fundamentals of Solid State Thermoelectric Cooling

In this section a few fundamental concepts of thermoelectric cooling are presented which will help lead up to the hypothesis regarding the feasibility of this project. Thermoelectric cooling is based on the Peltier effect. This effect, discovered by Jean-Charles Peltier in 1834, states that when an electric current is driven through a junction between two different conductors heat is absorbed or generated, depending on the direction of current flow. The amount of heat transferred depends on the materials used to form the junction [7, 8]. Extensive research has been conducted in the last few decades to develop materials that exhibit thermoelectric properties strong enough to be of practical value [9, 10]. Today's commercially available thermoelectric modules use tightly arranged pellets of bismuth telluride, and are capable of pumping almost 10 watts/cm^2. Fig. 4 shows a simplified diagram of such a TEC module. Fig. 4(a) represents a thermoelectric single junction and shows the flow of electric current and heat. Fig. 4(b) shows how several of these thermoelectric junctions are assembled to make a TEC module.

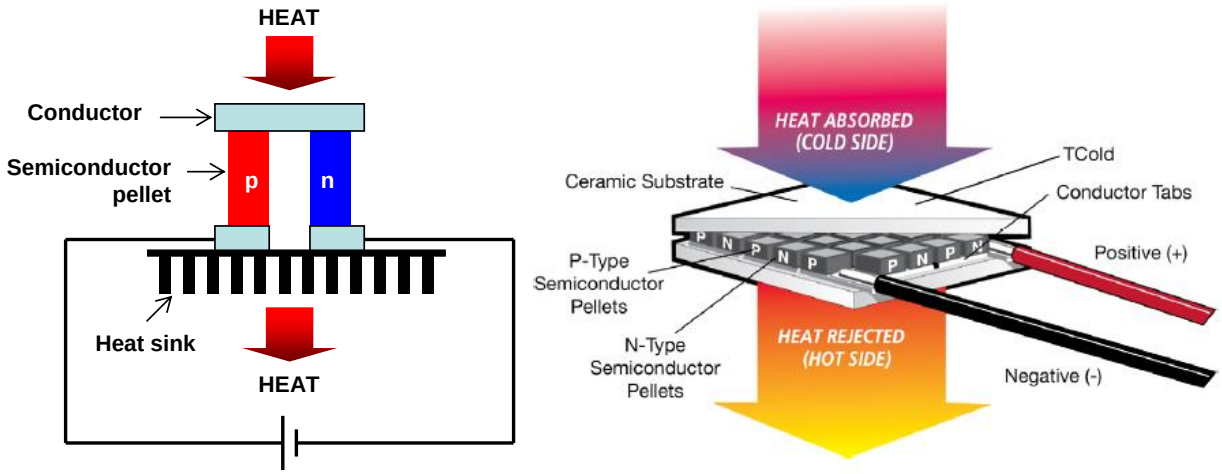

(a) (b)

Fig. 4. Simplified diagram of a TEC showing (a) a single junction and (b) an assembled view of a TEC module.

The Coefficient of Performance (COP) of TEC modules depends on a "figure of merit" of the thermoelectric material used. This figure is denoted as *ZT* and is given as [7]:

$$ZT = \frac{\sigma \times S^2 \times T}{K}, \tag{6}$$

where σ is the electrical conductivity of the thermoelectric material, *S* is its Seebeck coefficient, κ is its thermal conductivity, and *T* is the average temperature of the TEC. For commonly used bismuth antimony telluride alloys the highest *ZT* is about 1. New superlattice materials can have

*ZT*s as high as 3.5 but these are not commercially available [9]. The dependence of maximum achievable COP of a TEC module on *ZT* is given by [6]:

$$COP_{\max} = \left[\frac{T_C}{T_H - T_C}\right]\left(\frac{\sqrt{ZT+1} - T_H/T_C}{\sqrt{ZT+1}+1}\right), \quad (7)$$

where T_H is the hot side temperature and T_C is the cold side temperature in Kelvin (degrees Celcius + 273). From equation (7) it is seen that if T_H and T_C are almost equal, then very high COPs are possible in theory [11].

1.4 Self-Cooling Concept Used in This Project

Fig. 5 shows a conceptual view of the self-cooling approach used in this project. The main reason for the rise in solar cell temperature is the infrared (IR) content in sunlight. This part of the solar spectrum is absorbed by the cell but cannot be used to generate electricity. Rather it increases cell temperature. The central idea of this project is to divert a small portion of the power generated by the solar cell to a high efficiency heat pump which will remove the IR energy. As a result, it is expected that the cell temperature will not rise as much as in the conventional non-cooled case, which is turn will result in a higher power output. The increase in cell power output must of course be larger than the power diverted to the heat pump in order to realize a net improvement.

The heat pump used in this work is of course a TEC module. As mentioned earlier, TECs operate very efficiently under low heat loads and low temperature differentials. These conditions are met very adequately since the objective here is to maintain the cell temperature at or near ambient air temperature, and since the IR energy content in sunlight presents a very modest head load. The applicability of TECs is discussed in more detail in Section 2.

The diversion of a fraction of the solar cell's output power to its own cooling module is implemented using a switching scheme. Such a method allows control over the amount of solar power being used for self-cooling and can be adapted based on environmental conditions and realized net power gain. Details of the actual implementation of this scheme are given in Section 3.

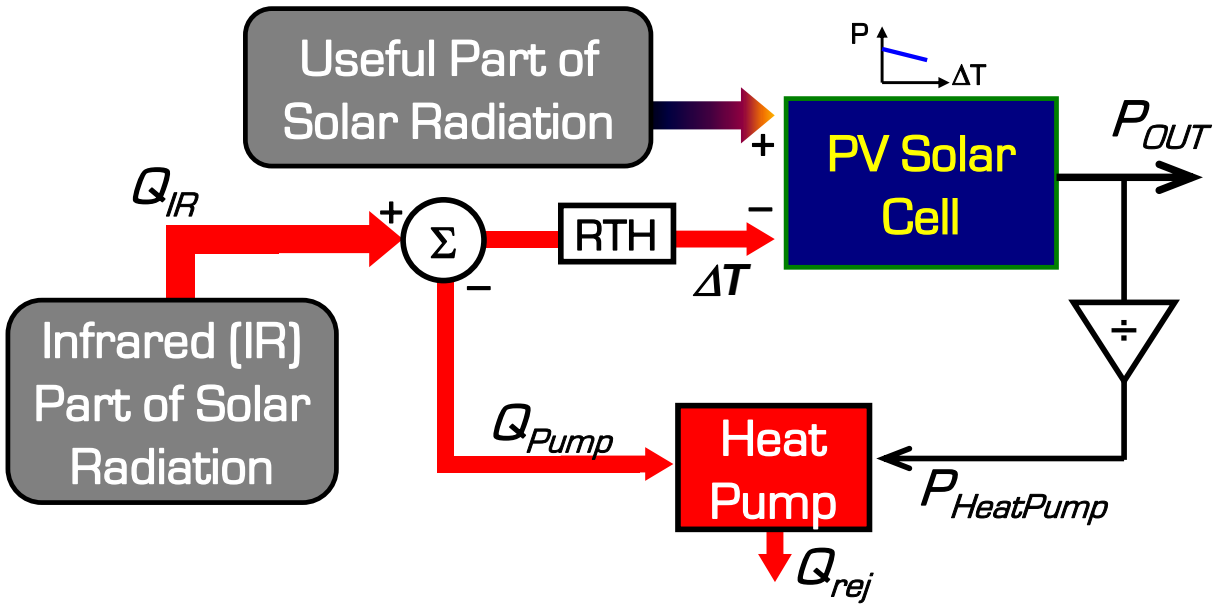

Fig. 5. Conceptual view of self-cooling approach used in this project.

1.5 Review of Prior Work

A review of the literature revealed only one prior work on self-cooled solar cells. This was reported by a team from Stanford University. The authors used radiative cooling to passively lower the temperature of solar cells operating under direct sunlight [12]. The basic idea used was to place a thin pyramid shaped silica layer that is transparent over solar wavelengths but strongly emissive over thermal wavelengths on top of the solar cell as shown in Fig. 6. Such a layer does not degrade the optical performance of the solar cell, but generates significant thermal radiation that results in solar cell cooling by radiatively emitting heat to outer space. A lowering of operating temperature of 18°K was reported. However, the results were based on computer simulations only and the effect on actual solar cell operation was not provided.

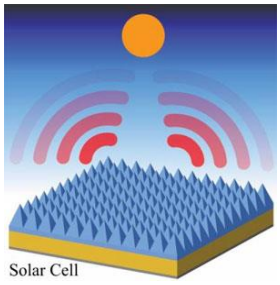

Fig. 6. Diagram of self-cooled solar cell developed by Stanford University team [REF].

2. Theory

2.1 Feasibility - Requirements from Theoretical Considerations

In this section the feasibility of improving power output a solar cell using self-cooling is considered from a theoretical aspect. This leads to requirements that must be satisfied in order for a successful realization of the project goals.

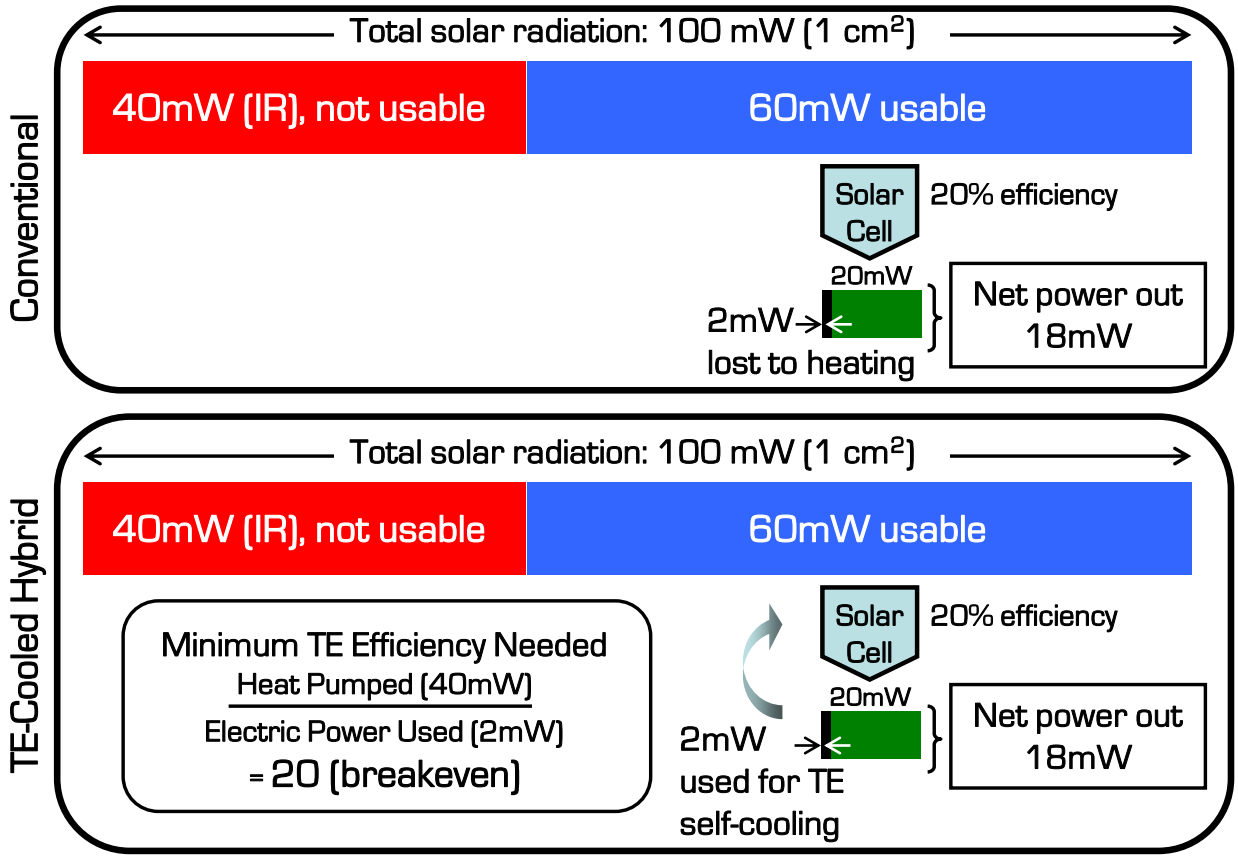

Fig. 7. Pictorial representation of power distributions leading to TEC COP requirement.

First, using (5) and assuming a 20°C increase in panel temperature under sunlight, it is seen that the peak power drops by about 10%. Next, assuming the use of a 20% efficient solar cell, solar radiation intensity of 100 mW/cm^2, and, for simplicity, an effective area of 1 cm^2, the ideal solar power output is 20 mW. Given the 10% loss in power output due to temperature rise, the actual power output drops to 18 mW, i.e. 2 mW is lost due to heating. However, if using 2 mW of power a heat pump could lower the cell temperature back to ambient level then the cell output would increase back to 20 mW and a "break-even" situation would be attained. If this

effect could be achieved with less than 2 mW power used by the heat pump, a net increase in power output would be realized.

Next, it is assumed that 40% of the solar radiation is IR and this is what the heat pump needs to remove. Continuing with the assumption of 1 cm^2 effective area leads to a heat load of 40 mW. Thus, it is seen that if with 2 mW of input electric power the heat pump could remove 40 mW of IR heat power, a break-even condition could be reached. This implies a COP of 20 or better would be needed for this approach to be feasible. Fig. 7 is a pictorial view of the arguments presented above.

2.2 Thermoelectric Heat Pump Performance

In this section the performance of TEC cooling modules is considered from a theoretical angle to determine under what conditions, if any, the COP requirement derived in the previous section can be met.

The cooling power at the cold end of a single stage thermoelectric cooling module is given by [10]:

$$Q_p = 2N\left(SIT_C - \frac{1}{2} I^2 \frac{\rho L}{A} - K\Delta T \frac{A}{L} \right), \tag{8}$$

where N is the number of thermoelectric junction pairs, S is the Seebeck coefficient of the thermoelectric material, I is the current through the thermoelectric module, T_C is the cold side temperature, ρ is the resistivity of the thermoelectric material, A is the cross-sectional area of each thermoelectric pellet, K is the thermal conductivity of the thermoelectric material, and ΔT is the temperature difference between the hot and cold sides of the TEC. The first term inside braces is the heat removed by the Peltier effect. The second and third terms represent, respectively, the heat injected into the cold side due to the electrical resistance of the TEC and heat conduction through the TEC from the hot side. These two latter effects tend to reduce the cooling power of the TEC.

Under steady temperature conditions the above cooling power is balanced by the heat load, which consists of any sources of heat, plus conduction of heat from the surrounding through the enclosure. This can be expressed as:

$$Q_{load} = Q_{gen} + K_W \Delta T\,, \tag{9}$$

where Q_{gen} represents heat generated by external heat sources such as sunlight. K_W is the effective thermal conductivity of the enclosure.

From equations (8) and (9) the temperature of the solar cell placed on the cold side of the TEC can be solved as:

$$T_C = \frac{Q_{gen} + N\rho(L/A)I^2 + \{K_W + 2NK(A/L)\}T_H}{2NSI + \{K_W + 2NK(A/L)\}}. \quad (10)$$

The total rate of energy consumption by the TEC (Q_{TE}) is the sum of Q_p and the rate at which heat is generated within the TEC due to its electrical resistance. It is given by [10]:

$$Q_{TE} = 2N\left(I^2 \frac{\rho L}{A} + SI\Delta T\right). \quad (11)$$

Lastly, the COP is given by the ratio of Q_p/Q_{TE}. Using equations (4) and (7) the COP is expressed as follows:

$$COP = \frac{SIT_C - \frac{1}{2}I^2 \frac{\rho L}{A} - K\Delta T \frac{A}{L}}{SI\Delta T + I^2 \frac{\rho L}{A}}. \quad (12)$$

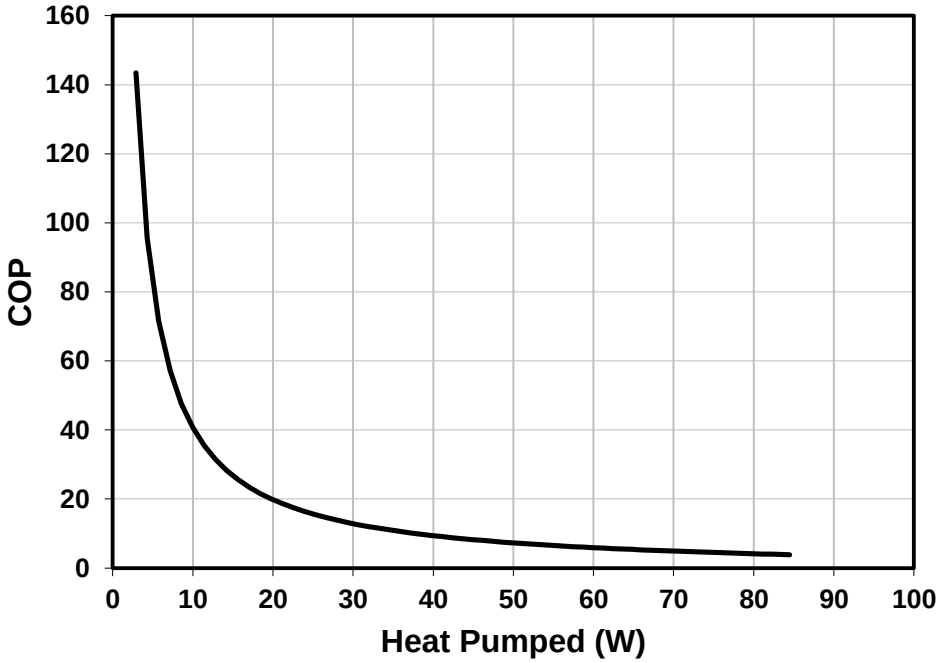

Fig. 8. Theoretically calculated COP versus heat load for a typical TEC module.

Fig. 8 shows a plot of *COP* as a function of heat load with zero ΔT, as computed from the equations above. The following values, which are typical of commercially available TECs, were

used for the various quantities in the equations: S = 2x10^{-4} V/K, K = 3 W/mK, N = 241, ρ = 2.5x10^{-4} ohm-cm. T_H was taken to be 27°C (i.e. 300K). It can be seen that at low heat loads the theoretical COP can be extremely high. In reality, it is unlikely that such high COPs can be realizable, but it appears from this analysis that there is sufficient theoretical support to believe that the goals of the project are realizable using the planned approach.

2.3 Hypothesis

Based on the theoretical discussion presented above it is hypothesized that the goal of the project, i.e. to demonstrate a thermoelectrically self-cooled that has a 5% (or higher) power output than a conventional cell, can be achieved provided the TEC modules can be operated at a low enough heat load (e.g. below 10W for the size of a module with 241 pellets) such that a COP greater than 20 can be maintained.

3. Design and Construction of Experimental Apparatus

In this section the various aspects of designing and building the experimental apparatus are described. In Section 3.1 the mechanical aspects of the design are considered, in Section 3.2 the electrical design and assembly are described, and lastly in Section 3.3 the software used for temperature self-regulation is described.

3.1 Mechanical Implementation

The single most critical factor in the mechanical design is thermal coupling between the TEC modules and the solar cell. It is essential that the best possible thermal contact between the solar cell and the TEC is achieved. The main difficulty with this is that the surface of TEC modules is composed of ceramic material to which a Si solar cannot be thermally bonded. Additionally, the bottom surface of the solar cell is its positive terminal and good electrical contact to the bottom surface is essential. To work around these difficulties the arrangement shown in Fig. 9 was used. The solar cell is soldered to a thin copper plate. The copper plate and a second aluminum plate are then clamped using high tension spring clamps with the TEC modules between them. Silver paste is applied to both surfaces of the TEC modules to improve thermal coupling with the copper and aluminum plate. Foam insulation is placed between the TECs to ensure no heat entry from the edges. Electrical contact is made by bolting a thick gauge wire to the copper plate on one side and a set of point contacts passing through the acrylic over on the other side. Fig. 10 shows a photograph of the completely assembled hybrid cell.

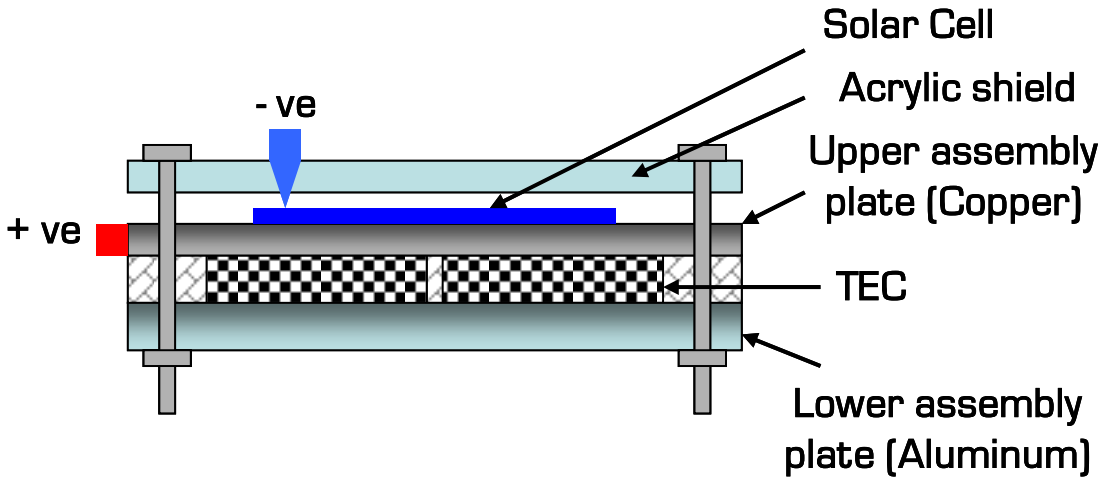

Fig. 9. Diagram showing details of how the self-cooled solar cell is assembled.

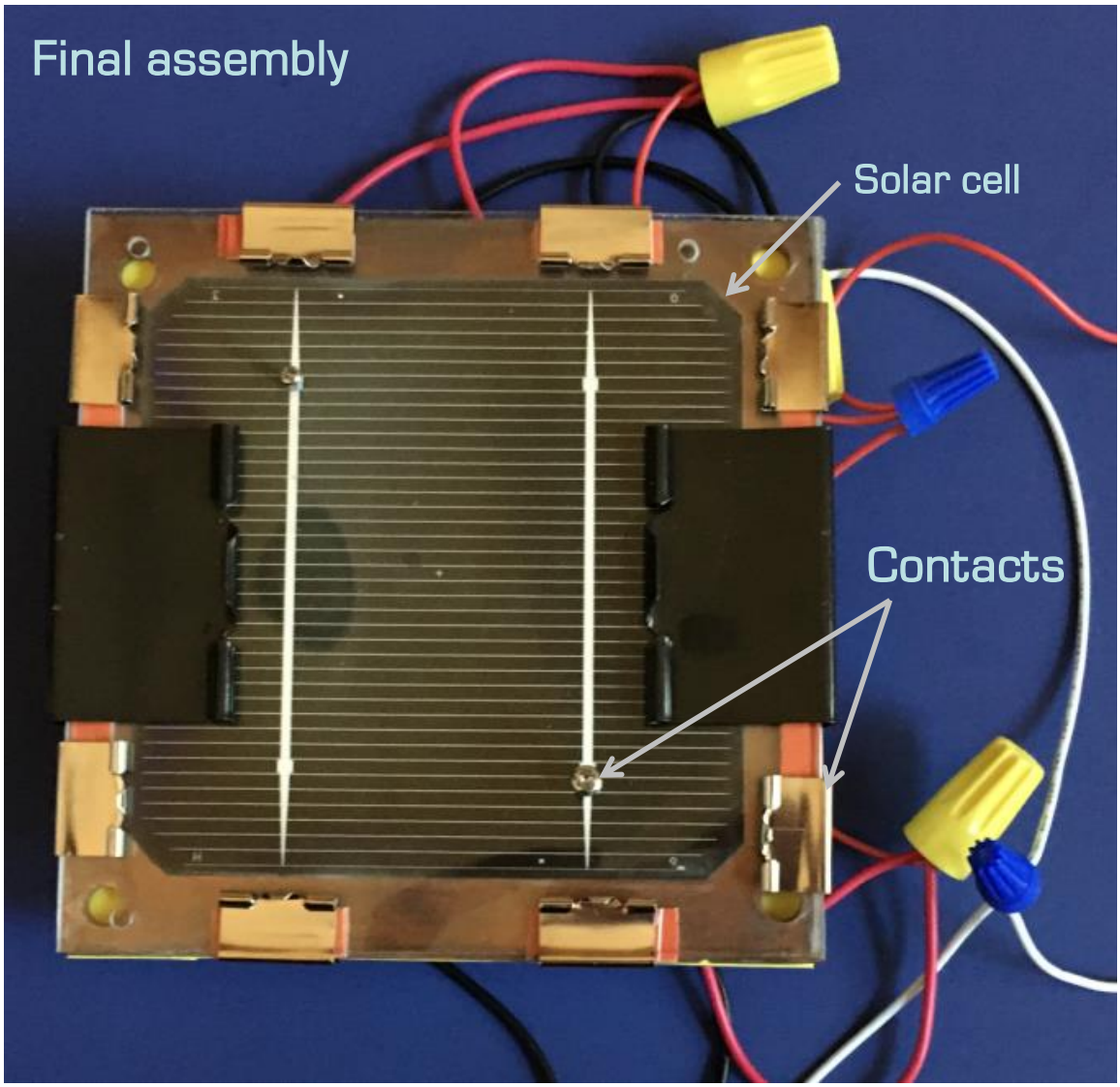

Fig. 10. Photograph of final assembled thermoelectrically cooled solar cell.

3.2 Electrical Implementation

As described earlier self-cooling is conceptually implemented by diverting a small portion of the solar cell's own power to the TEC modules. The real implementation of this was achieved using a switching circuit. Referring to Fig. 11, two switches S1 and S2 are used to shift the solar cell's output periodically to the load for a certain time duration and the TEC modules for the remainder time duration of the period. The fraction of the switching time period for which the actual load is driven is called the duty cycle D. Obviously, then (1-D) represents the fraction of the time period for which the TEC module is driven by the solar cell.

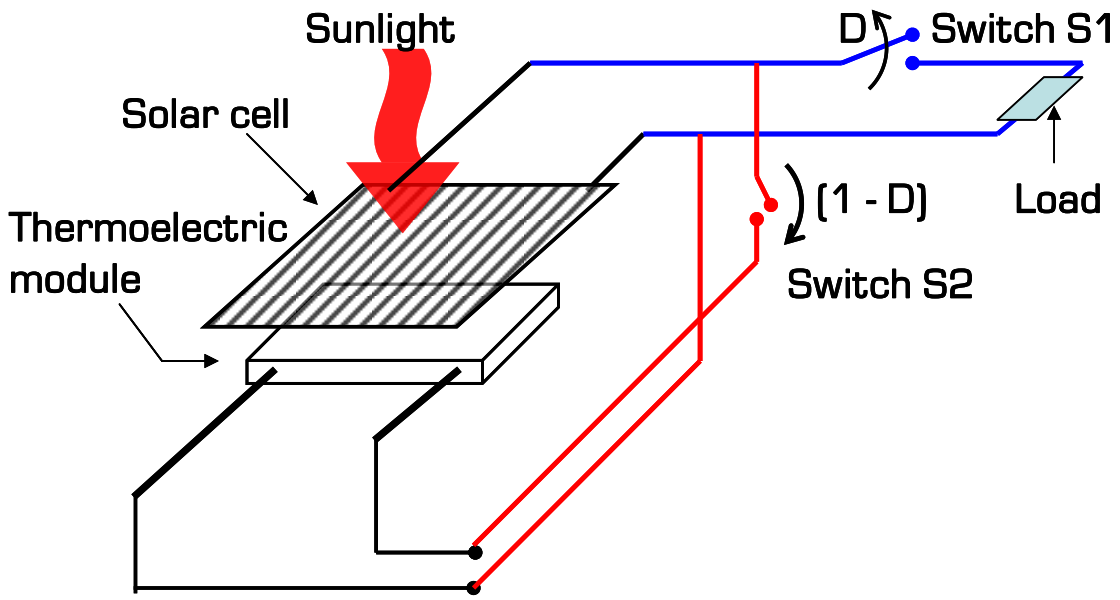

Fig. 11. Conceptual schematic of switching circuit used to divert a portion of the solar cell power output to the thermoelectric cooling module.

Fig. 12 shows the next level of detail in the implementation of the switching circuit. The switches S1 and S2 are implemented using MOSFETs. MOSFETs are semiconductor devices which can be turned on or off using an electrical signal (a voltage) applied to its gate terminal. When the gate signal goes high the MOSFET behaves like a closed switch, and when the gate is low the MOSFET behaves like an open switch. The gate driver block shown in Fig. 12 represents a circuit which generates the gate signals that turn the MOSFETs on or off in a complementary fashion, i.e. when one turns on the other turns off and vice versa. The capacitor C2 shown in Fig. 12 is a "charge bucket" that supplies the load when switch S1 is open. This helps reduce the ripple across the load. To minimize the ripple it is important to keep the absolute value of the off-time of S1 small.

Fig. 13 shows further details of the gate driver circuit. The gate driver is implemented using a dual 555 timer integrated circuit. The first 555 generates a pulse train whose duty cycle is determined by the values of R1, R2, and C1. The second 555 generates a complementary copy of the first pulse train. The duty cycle D is varied by changing the value of R1. The exact relations between the component values and the on time, off time, and duty cycle are given below.

$$t_{ON} = 0.693(R1 + R2)C1 \tag{13}$$

$$t_{OFF} = 0.693R2C1 \tag{14}$$

$$D = \frac{t_{ON}}{t_{ON} + t_{OFF}} = \frac{(R1 + R2)}{R1 + 2R2} \tag{15}$$

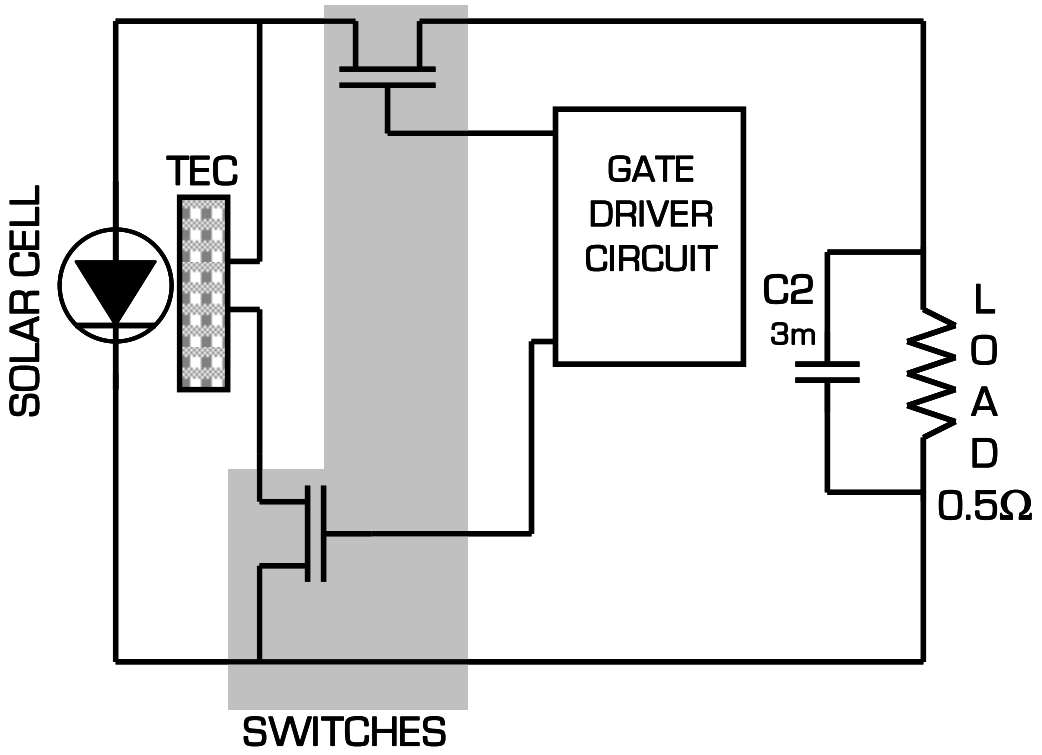

Fig. 12. Diagram showing circuit used to monitor power generated by solar cells.

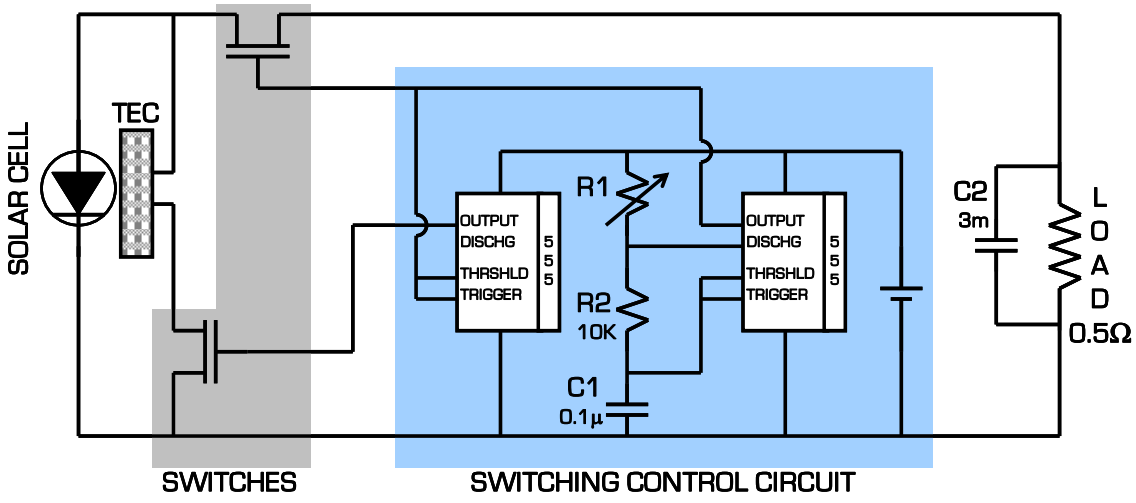

Fig. 13. Circuit schematic showing details of gate driver circuit implementation using 555 timers.

As shown in Fig. 13, the component values used in the circuit design are R2 = 10K, and C1 = 0.1μF. For R1, a potentiometer (variable resistor) was used to study the effect of duty cycle on power output. However, for a adaptively self-regulated solar cell design R1 was implemented in a way that allowed it to be varied amongst four preset discrete values based on the difference between cell temperature and ambient air temperature.

An Atmel Atmega168 8-bit microcontroller was used to digitally adjust the value of R1 and thereby the duty cycle. Two type-K thermocouple temperature sensors were used to detect the temperatures of the solar cell and the ambient air. The thermocouple outputs were fed to the analog to digital (ADC) inputs of the microcontroller. The microcontroller software was written to compute the difference between cell and air temperature and depending on the magnitude of the difference, set one of four bits of the output port B low. The pins of the output port B were connected to four p-channel MOSFETs. The MOSFET connected to the low bit turns on activating the resistance in series with it. Fig. 14 is a schematic of the duty cycle control circuit.

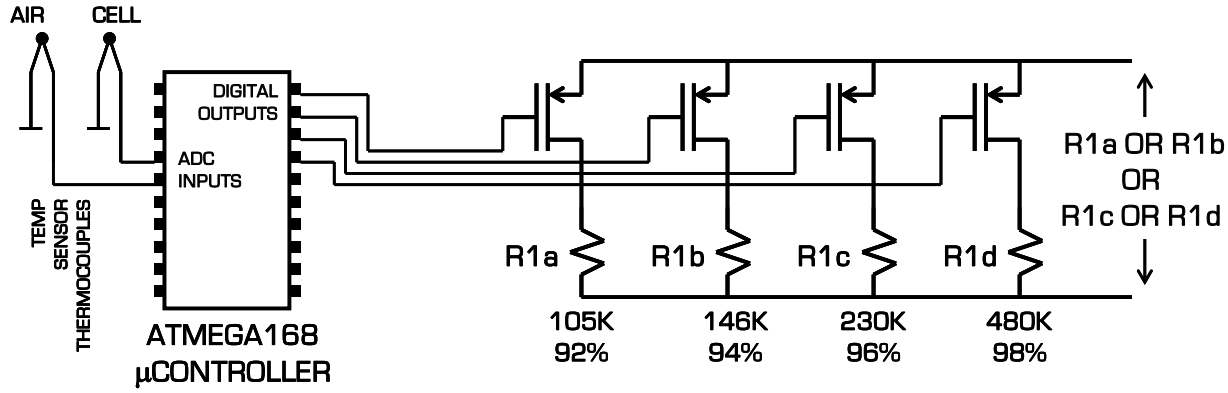

Fig. 14. Schematic drawing of the digital duty cycle control circuit.

3.3 Software Implementation

The software code used in the microcontroller to adjust duty cycle is written in c. The code consists of an initialization function, a function to read the ADC output, and a main function that sets the port B bits depending on the sensed temperatures. The entire code is given in Appendix A. Fig. 15 shows a photograph of the entire setup.

INSERT Fig. 15!!

4. Experimental Results

4.1 Preliminary Measurements on Conventional Solar Cell

The first experiment is done to examine the I-V behavior of the solar cell in use and determine the optimum load that will result is maximum power delivered from the solar cell. Fig. 16 shows the I-V behavior measured under natural sunlight. The various points are obtained by changing the load resistance. The open circuit voltage is about 0.575 mV and the short-circuit current is just over 1 amp. The maximum power draw is at Vcell=0.49, I = 0.7A. The voltage across the load at this point is 0.35V indicating a series resistance of 0.2 ohms due to the wiring. From this data it is also concluded that the optimum load resistance for the cell and measurement apparatus in use is about 0.5 ohms. All subsequent comparative experiments were done with this load.

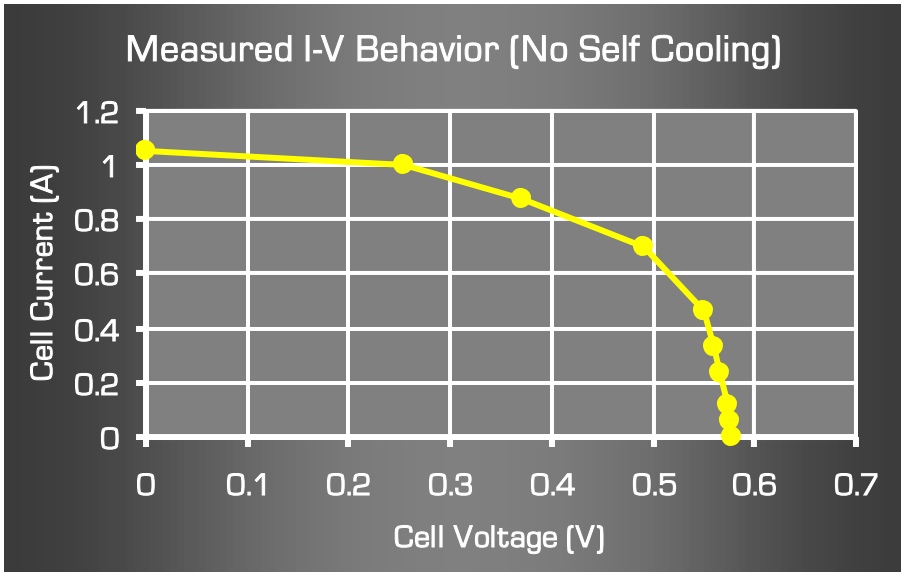

Fig. 16. Measured I-V behavior of a conventional solar cell used to locate the maximum power point.

Next, the effect of cell temperature rise due to solar radiation is measured. Fig. 17(a) shows the measured open-circuit voltage (Voc) degradation over time in a conventional solar cell with no cooling. There is about a 50mV decrease over a two-hour period. Fig. 17(b) shows the cell's temperature variation of over the same period. There is about a 20°C increase in temperature. The resultant loss in peak power output is about 10% of the original power.

The last measurement of this section is a check of the gate driver signals. The key requirement is for the gates of the MOSFETs implementing switches S1 and S2 to turn on and off synchronously. Fig. 18 shows the measured gate drive signals. They are as designed.

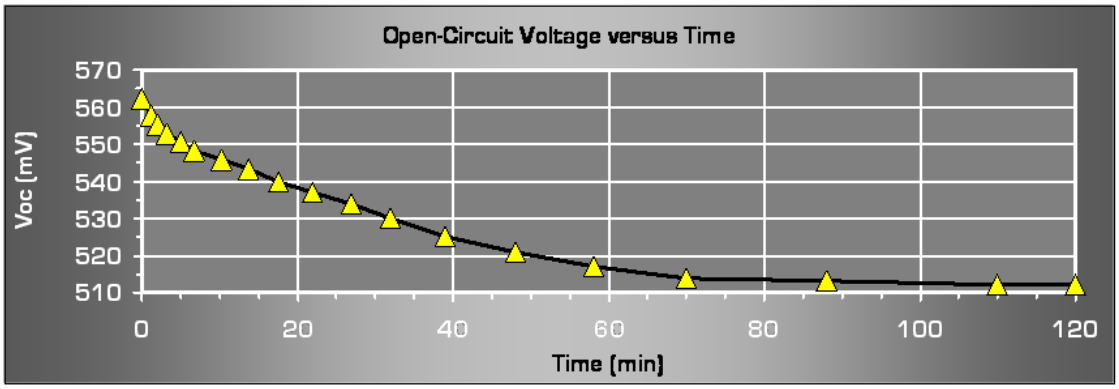

(a).

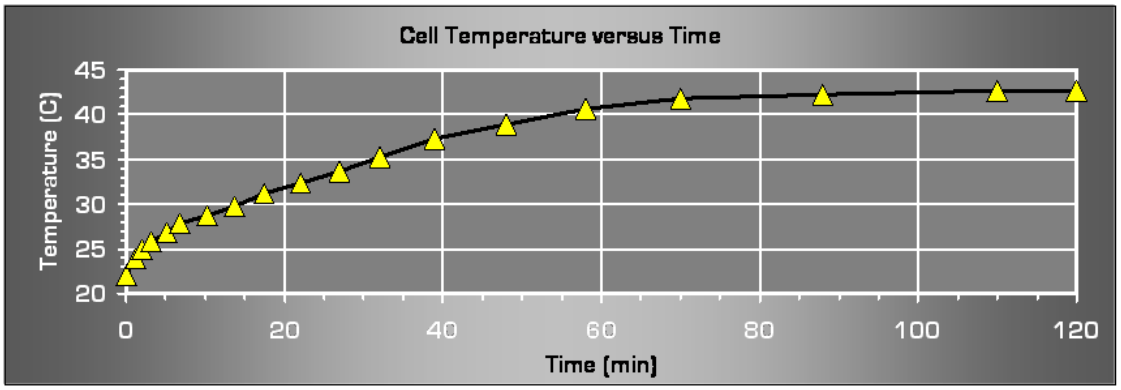

(b)

Fig. 17. (a) Open-circuit voltage and (b) temperature versus time for conventional solar cell.

Fig. 18. Oscilloscope waveform of gate drive signals showing correct complementary switching.

4.2 Power Output versus Duty Cycle Without Cooling

The power versus duty-cycle behavior of the solar cell with the TEC modules disconnected is examined in this section. This set of measurements is done for reference only. As mentioned previously, a 0.5 ohm load resistor is used to draw maximum power from the solar cell. Duty cycle is varied by changing R1 manually. Voltage waveforms across the load are measured using a Rigol DS1052 digital oscilloscope.

Fig. 19 shows the voltage waveform across the load resistance for several duty cycles. It is seen that the voltage across the load does not drop to zero during the portion of the switching cycle when the power to the load is cut off. This is because the capacitor C2 holds the output voltage and prevents it from dropping all the way to zero. As a result, there is only a small ripple around the switching points.

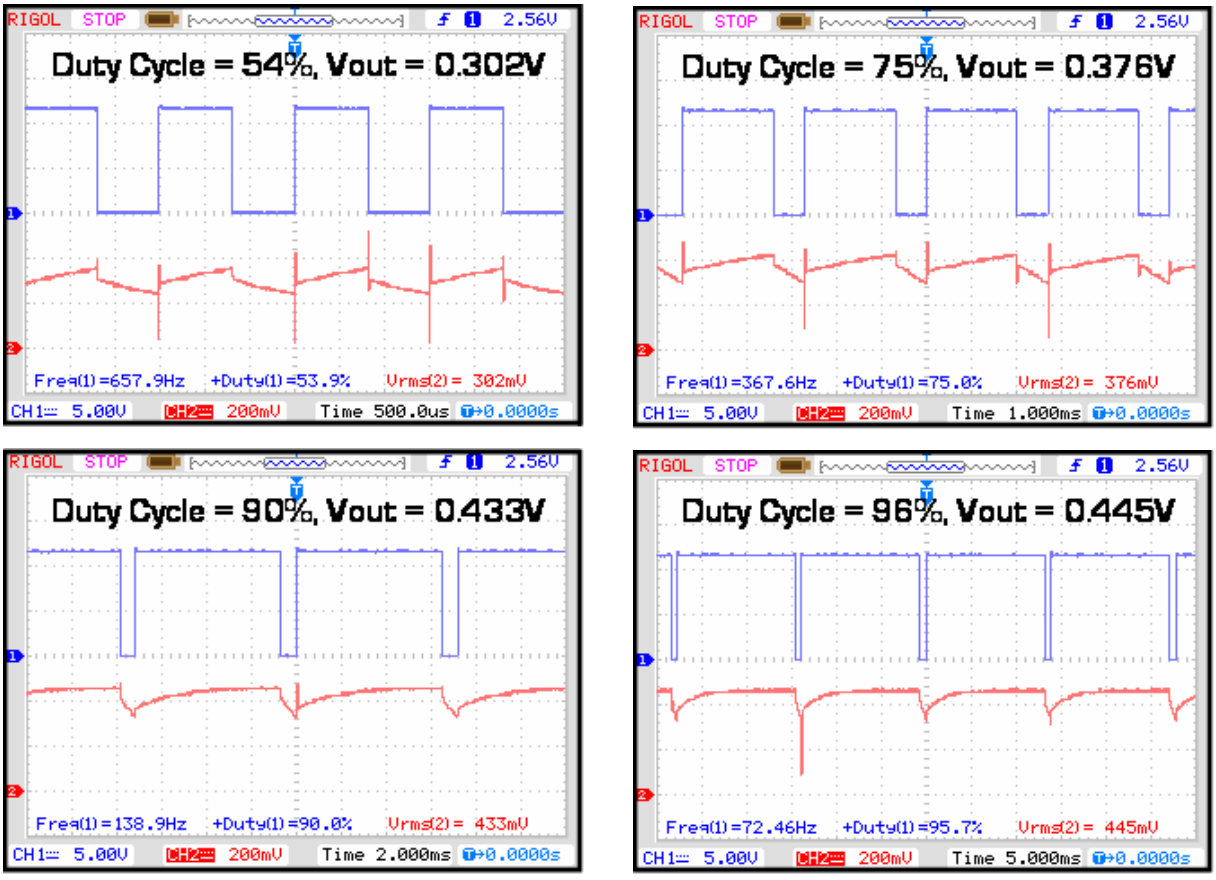

Fig. 19. Voltage waveforms across load (bottom) and gate signal S1 for various duty cyles.

Fig. 20 shows the power versus duty cycle behavior without cooling. Power delivered to the load was calculated using the RMS voltage reported in each case by the oscilloscope. As seen, there is a linear relation between power and duty cycle. This is exactly as expected from theory.

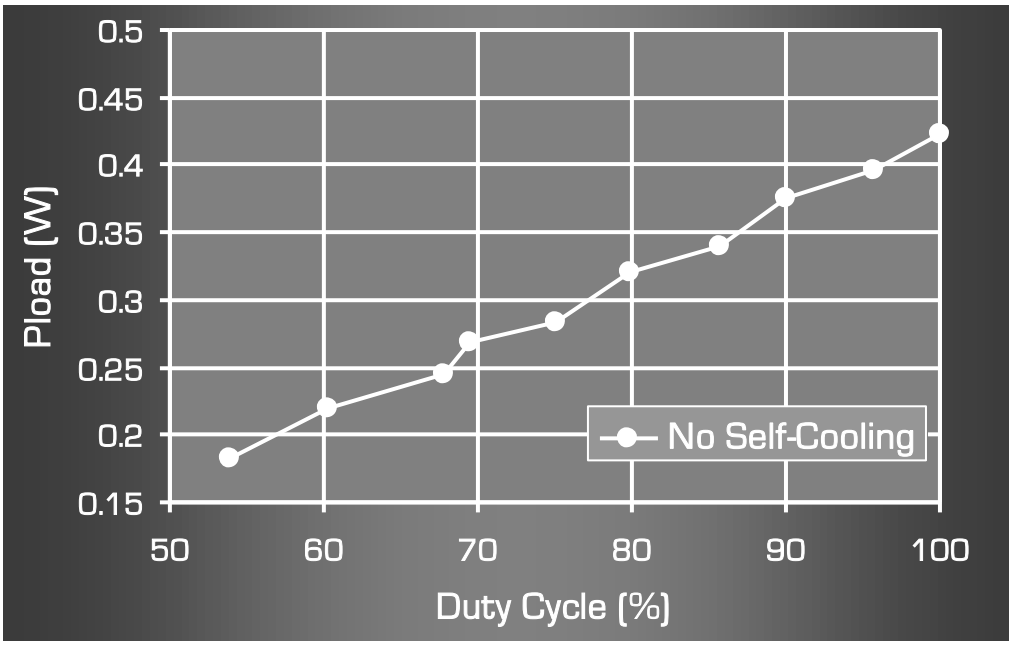

Fig. 20. P Power output versus duty cycle with the TEC module disconnected.

4.3 Power Output versus Duty Cycle With Thermoelectric Self-Cooling

The power versus duty-cycle behavior of the solar cell with the TEC modules connected is examined in this section. As before, a 0.5 ohm load resistor is used to draw maximum power from the solar cell. Duty cycle is varied by changing R1 manually.

Fig. 21 shows the voltage waveform across the load resistance for several duty cycles. As in the previous experiment, because of the presence of capacitor C2, there is only a small ripple around the switching points. Fig. 22 shows the power output as a function of duty cycle. Unlike the previous case, as the duty cycle is lowered slightly from 100% the power output of the cell increases. With further decreases in duty cycle the power output begins to drop. At around 90% duty cycle the advantage from self cooling drops to zero. At the peak output, which occurs at about 96% duty cycle, the solar cell output is 10.25% higher than without self cooling. Thus the primary objective of the project is met.

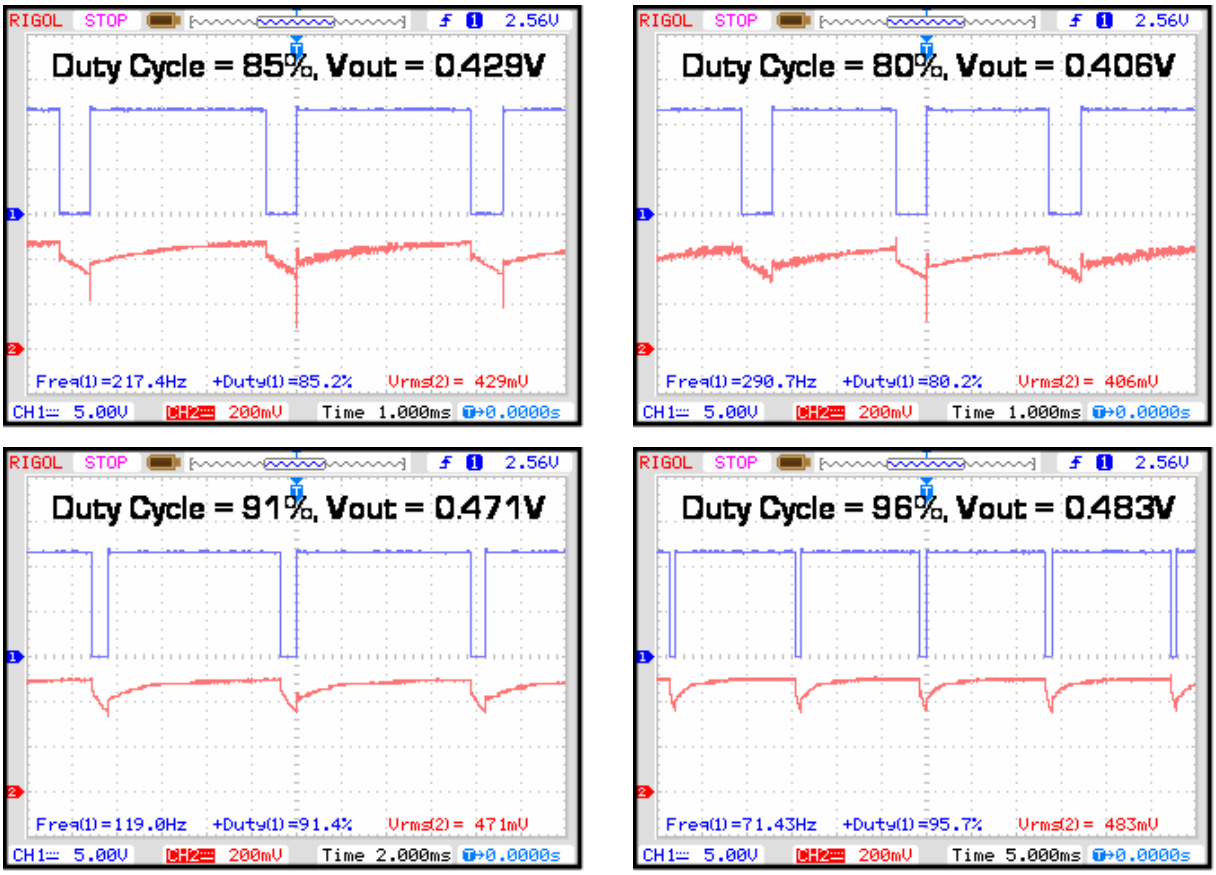

Fig. 21. Voltage waveforms across load (bottom) and gate signal S1 for various duty cyles with self-cooling on.

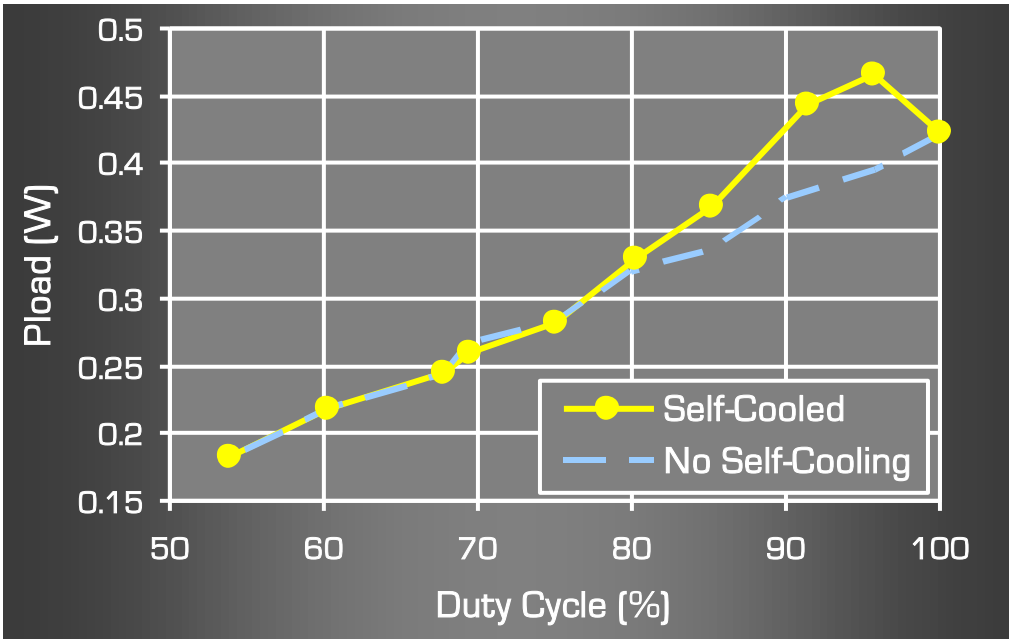

Fig. 22. Power output versus duty cycle in a self-cooled solar cell. Power output peaks at about 96% duty cycle. At this duty cycle the power output is 10.25% higher than without cooling.

4.3 Thermoelectric Self-Cooling with Auto Adjusting Duty Cycle

In this section measurement results are presented for the case where the solar cell operates autonomously, i.e. it adjusts the switching duty cycle automatically depending on the difference between the temperatures sensed at the cell itself and the ambient air.

The power delivered to a 0.5 ohm external load resistor was measured under natural sunlight with the cell in auto adjusting self cooling mode. Measurements were recorded every 15 minutes from 11:00 am to 3:00pm. For comparison, the same measurements were repeated without self cooling. Fig. 23 shows the results. It can be seen that the self-cooled cell produces more power at almost all time points. As the air temperature increased there was a drop in the open circuit voltage, but because of the simultaneous increase in sun angle, the short circuit current also increased. Because of these two opposite effects the overall variation in power output over the four hour measurement period was quite uniform. Of course, the self-cooled cell produced more power consistently.

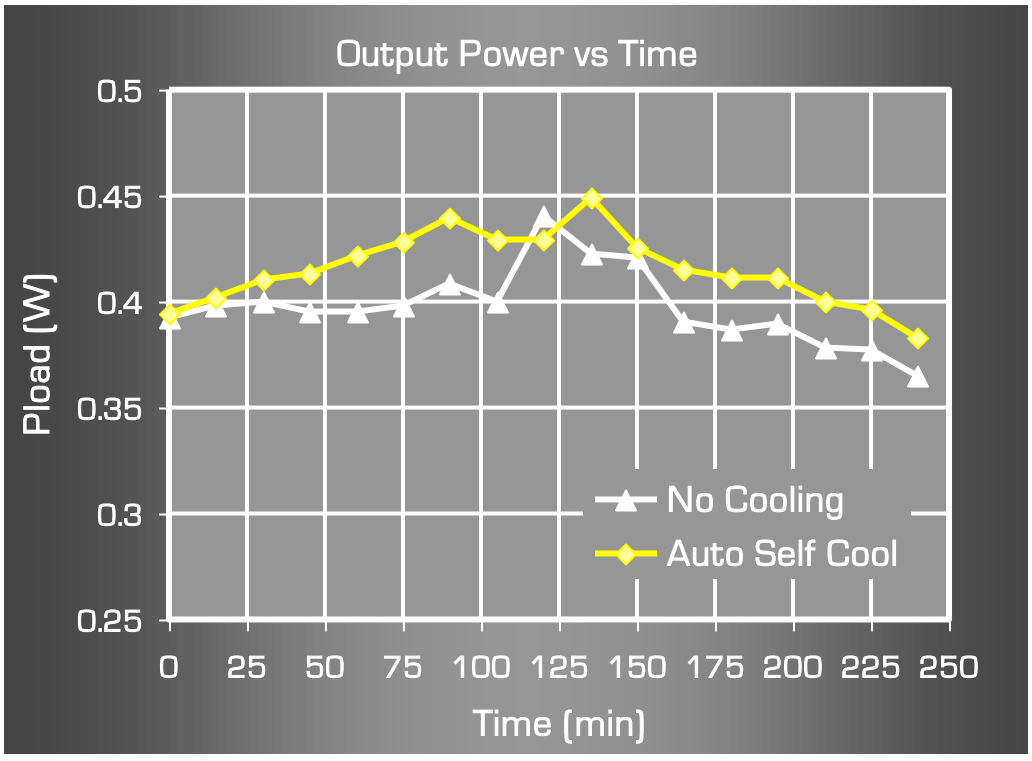

Fig. 23. Variation of power output over time for both conventional and self-cooled solar cell.

6. System Cost Comparisons

The cost associated with a photovoltaic solar power system is not just the cost of the solar cells or solar panels. Aside from panel cost, there a number of peripheral costs that needs to be taken into account. Peripheral costs include the price of land, wiring, harnessing, power conditioning, storage for night-time use, etc. As a matter of fact, at today's market prices, on a per watt basis, peripheral costs comprise about 75% of the total installation cost of a practical solar power system and only 25% is related to the cost of the solar cells themselves. Clearly then if the power output of solar cells can be improved, then significant reductions in system cost can be realized. However, it is only natural that solar cells that have higher efficiencies and produce more power will cost more. At the same time though, it is entirely conceivable that the higher cell cost can be more than offset by reductions in peripheral cost (e.g. less land, wiring, etc. will be needed to produce the same power if each cell can output more energy.)

More analytically, the price of solar cells as a function of its power output capacity can be expressed as:

$$C_{CELL} = C_{C0}\left(e^{P/P_0} - 1\right), \tag{13}$$

where C_{C0} and P_0 are fitting parameters. This expression is an empirical fit to market data obtained for a few commercial solar cells of varying efficiencies. The fit of the expression of equation (13) to this data is shown in Fig. 24a. Similarly, the peripheral cost can be expressed as

$$C_{PERI} = C_{P0}\frac{P_B}{P} \tag{14}$$

where C_{P0} is also a fitting parameter. Combining the two opposite effects of (13) and (14) results in a relationship between cost per watt and cell power output as shown in Fig. 25. It is seen that beyond a certain point, increasing cell power output becomes prohibitively expensive in terms of CPW. Additionally, to be cost competitive with fossil fuels solar power CPW has to drop by about 30%. This graph implies that will require a 25% increase in cell power output (and assumes a corresponding increase in cell cost).

Table 1 shows a cost analysis of the self-cooled solar cell developed in this project. The bottom line is that the 10.25% improvement in power output resulted in an approximately 5% decrease in CPW. This not only meets the project's secondary objective, but is also in line with the analysis presented above.

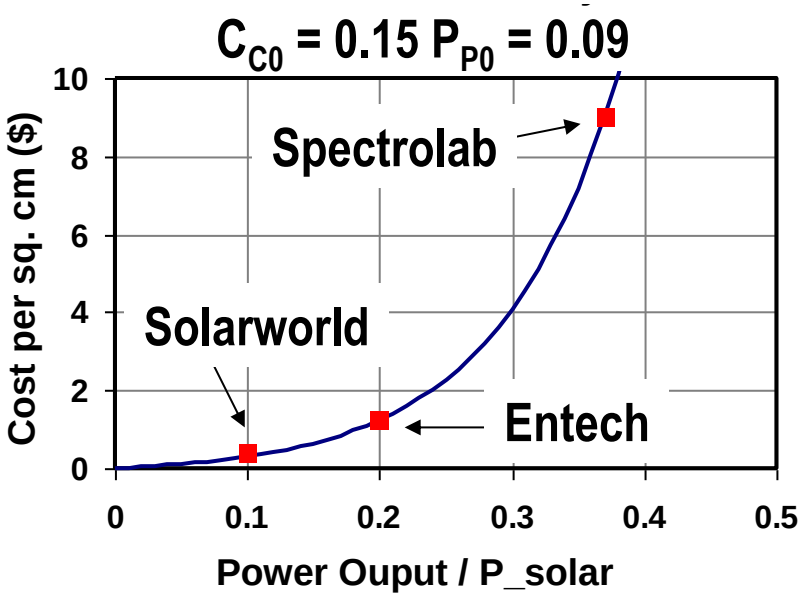

Fig. 24. Model of solar cell cost as a function of cell's output power capacity.

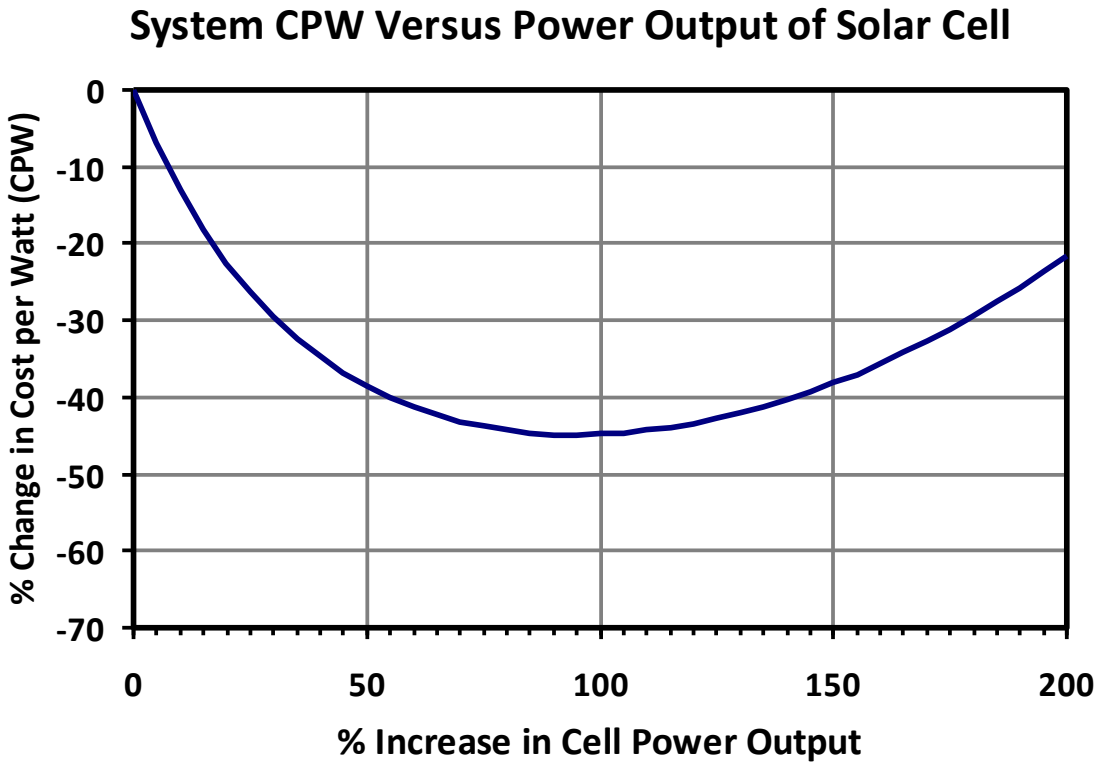

Fig. 25. Analytically modeled variation in the change in CPW as a function increase in cell output power.

Table 1.Cost analysis of self cooled solar cell developed in this project.

Type of cell	Cell Cost ($)			Peri. Cost ($)	P_{out} (W)	CPW ($/W)
	PV	TE Module	Total			
Conventional	1.25	n/a	1.25	3.75	0.423	11.8
TE Cooled Hybrid	1.25	0.06*	1.31	3.93	0.467	11.2

5. Discussion

It is well known that solar cells can provide a source of clean energy. However, the cost of solar energy is still too high for it to be a viable alternative to fossil fuels. Most projects on solar cells attempt to increase the power output of these cells without considering the increases in cost. The results tend to be economically unusable. This project demonstrates a practical method to reduce the cost per watt of solar power, by SIMULTANEOUSLY optimizing the power output and cost of a solar cell. It was possible to come up with a way to make solar energy more cost competitive with energy from fossil fuels. By analyzing the factors that affect cost per watt of a solar cell, it was determined that by increasing the power output of a typical conventional low-cost cell by about 5% while limiting the associated cost increase to about 15% could bring the cost of solar closer to fossil fuels. Solar cells lose about 10% of their power output due to heat from sunlight. This is due to the sensitivity of its open circuit voltage to temperature. Thermoelectric cooling was used in an innovative way to recover a large portion of this power loss.

Thermoelectric cooling is very efficient at low heat loads and low temperature differentials. There are the exact conditions that solar cells operate in. The cost of TE modules has also dropped significantly in recent years, making this a very cost effective option. After theoretically testing the validity of these hypotheses, an innovative system was constructed that used a digitally controlled switching circuit to utilize a fraction of the solar cell's own power to control its temperature and thereby improve its power output. Several experiments were conducted to study quantitatively the improvements achieved using this technique. The objective was to increase the net power output of a solar cell by 5% compared with a conventional system. Experimental results showed that this was exceeded; an increase of 10.25% in power output was demonstrated using this new self-cooled cell.

Returning to the cost analysis, the hybrid system, when maintaining the TE module at the optimal point, the cost per watt of the hybrid TEC cooled cell is 5% lower than that of the conventional cell. The 10.25% increase in power output achieved results in a significant drop in cost per watt since we are operating on a portion of the characteristic that is highly sensitive to solar cell efficiency.

7. Future Work

The following lines of work are planned for the future.

(a) Study the effect of cascading multiple thermoelectric modules to further increase efficiency of hybrid cell [13, 14].

(b) Refine algorithms for adaptively controlling cooling power of thermoelectric modules with changing environmental conditions.

(c) Study the effect of concentrating sunlight.

(d) Investigate methods to optimize cost per watt of electricity generated using cost model.

8. Conclusions

In conclusion, the following comments are made to summarize the findings of this project.

1. Conventional solar cells lose efficiency due to temperature rise - this can be prevented using a thermoelectric (TE) based self-cooling technique.

2. Project objective of 5% increase in cell efficiency was exceeded with thermoelectric (TE) based self-cooling.

3. At the low heat loads of normal sunlight the coefficient of performance of thermoelectric modules can be very high.

4. Using an adaptive algorithm programmed into a microcontroller and a switching circuit with digitally controllable duty cycle, it was shown that a very stable increase in net power output of a solar cell can be attained.

5. Cost model relating cost per watt to design parameters was developed. It accounts for higher cost of TE cooled hybrid solar cell and shows that increased efficiency of TE cooled cell will allow the extra cost to be recovered in time.

9. References

1. Shockley, W. & Queisser, H. J., "Detailed Balance Limit of Efficiency of p-n Junction Solar Cells", *Journal of Applied Physics*, 32, pp. 510 – 519, 1961
2. De Vos, A., "Detailed Balance Limit of Efficiency of Tandem Solar Cells", *Journal of Physics D: Applied Physics*, 13, pp. 839 – 846, 1980
3. Corcoran, E., A, "Trick of the Light", *Forbes*, pp. 93, 94, 2007.
4. Honsberg, C. & Barnett, A., "Achieving a Solar Cell of Greater than 50 Percent: Physics, Technology, Implementation and Milestones", retrieved from University of California, Santa Barbara website: http://www.iee.ucsb.edu/event/solar-cell/.
5. Kirkpatrick, D., Eisenstadt, E., & Haspert, A., "DARPA Pushes for 50% Efficient Photovoltaics to Power Soldiers' Small Tools", *SPIE Newsroom*, pp. 1 - 2, 2006.
6. Sherif, R. A., King, R. R., Karam, N. H., & Lillington, D. R., "The Path to 1 GW of Concetrator Photovoltaics Using Multijunction Solar Cells", *Proceedings of 2005 IEEE Photovoltaic Specialists' Conference*, pp. 17 – 22, 2005.
7. Rowe, D. M., Editor, *CRC Handbook of Thermoelectrics*, CRC Press, 1995
8. Nolas, G. S., Sharp, J., Goldsmid H. J., *Thermoelectrics – Basic Principles and New Materials Developments*, Springer, 2001.
9. Li, J., Liu, W., Zhao, L., Zhou, M., "High-performance Nanostructured Thermoelectric Materials," *NPG Asia Materials*, vol. 2, pp. 152-158, 2010.
10. Harman, T. C., Walsh, M. P., laforge, B. E., Turner, G. W., "Nanostructured Thermoelectric Materials," *Journal of Electronic Materials*, vol. 34, pp. L19-L22, 2005.
11. Goldsmid, H. J., Douglas, H. W., "The Use of Semiconductors in Thermoelectric Refrigeration," British *Journal of Applied Physics*, vol. 5, pp. 386 - 390, 1954.
12. L. Zhu, A. Raman., K. Wang, M. Anoma, S. Fan, "Radiative Cooling of Solar Cells," *Optica* 1, pp. 32-38, 2014.
13. M. Olivares-Robles, F. Vazquez, and C. Ramirez-Lopez, "Optimization of Two-Stage Peltier Modules: Structure and Exergetic Efficiency," *Entropy*, vol. 14, pp. 1539 – 1552, 2012.
14. O'Brien, B. J., Wallace, C. S., Landecker, K., "Cascading of Peltier Couples for Thermoelectric Cooling," *J. Applied Physics*, 27, pp. 820 - 824, 1956.

APPENDIX A

The code used in the microcontroller to dynamically adjust the switching duty cycle is given below.

```
// tempsensor.c
// MCU = ATmega168

#define F_CPU 14745600
#define N_SAMPLE 200

#include <stdio.h>
#include <math.h>

#include <avr/io.h>
#include <avr/interrupt.h>
#include <avr/pgmspace.h>
#include <inttypes.h>

#include "../libnerdkits/delay.h"
#include "../libnerdkits/lcd.h"
#include "../libnerdkits/uart.h"

void adc_init() {
  // this function used to initialize A2D converter

  // set mux to use input at ADC0
  ADMUX = 0;

  // enable A2D converter by setting ADEN bit high
  ADCSRA = (1<<ADEN);

  // prescale clock to 1/128 for SAR resolution
  // ADPS bits set to 111 per data sheet for 1/128 scaling
  ADCSRA |= (1<<ADPS2) | (1<<ADPS1) | (1<<ADPS0);

  // run a single trial conversion by setting ADSC bit high
  ADCSRA |= (1<<ADSC);
}

uint16_t adc_read() {
  // this function reads output from ADC
  // returns an unsigned 16-bit integer

  while(ADCSRA & (1<<ADSC)) {
    // check ADSC bit, if high conversion is in progress
    // wait till any running conversion finishes
  }

  // merge results from ADCL/ADCH registers
  // ADC output is 10 bits wide, cannot fit in one register
  // ADCL must be read first (datasheet pp. 259)
  uint16_t result = ADCL;
  uint16_t temp = ADCH;
  result = result + (temp<<8);
```

```
  // fire next conversion
  ADCSRA |= (1<<ADSC);

  return result;
}

double genCelcius(uint16_t digLvl) {
  // ADC increment size = 5/1024 V
  // AD8495 thermocouple amp: T = (Vout - 1.25)/0.005
  // Output = (digLvl*increment - 1.25)/0.005
  return (digLvl * (5.0 / 1024.0) - 1.25) / 0.005;
}

int main() {
  adc_init();
  DDRB = 0b00011110;
  lcd_init();
  FILE lcd_stream = FDEV_SETUP_STREAM(lcd_putchar, 0, _FDEV_SETUP_WRITE);
  lcd_home();

  uint16_t adcRead = 0;
  double tempOut;
  double cellTemp, airTemp, dT, dutyCycle;
  uint8_t i;
  while(1) {
    // for stable result take average of a number of readings
    cellTemp = 0.0;
    for(i=0; i<N_SAMPLE; i++) {
      adcRead = adc_read();
      tempOut = genCelcius(adcRead);
      cellTemp = cellTemp + tempOut/N_SAMPLE;
    }
    ADMUX = 0b00000001;
    airTemp = 0.0;
    for(i=0; i<N_SAMPLE; i++) {
      adcRead = adc_read();
      tempOut = genCelcius(adcRead);
      airTemp = airTemp + tempOut/N_SAMPLE;
    }
    ADMUX = 0b00000000;
    dT = cellTemp - airTemp;
    if (dT > 8) {
      PORTB = 0b00010000;
      dutyCycle = 0.92;
    }
    else {
      if (dT > 6) {
        PORTB = 0b00001000;
        dutyCycle = 0.94;
      }
      else {
        if (dT > 4) {
          PORTB = 0b00000100;
          dutyCycle = 0.96;
        }
        else {
          if (dT > 2) {
```

```
            PORTB = 0b00000010;
            dutyCycle = 0.98;
          }
          else {
            PORTB = 0b00000000;
            dutyCycle = 1.0;
          }
        }
      }
    }

    // output results to LCD
    lcd_home();
    lcd_write_string(PSTR("Dig Lvl: "));
    lcd_write_int16(adcRead);
    lcd_write_string(PSTR(" of 1024 "));
    lcd_line_two();
    fprintf_P(&lcd_stream, PSTR("Cell:%.1fC Air:%.1fC"), cellTemp, airTemp);
    //lcd_write_data(0xdf);
    lcd_write_string(PSTR("C      "));
    lcd_line_three();
    fprintf_P(&lcd_stream, PSTR("Duty Cycle: %.2f"), dutyCycle);
    //lcd_write_data(0xdf);
    //lcd_write_string(PSTR("C"));
    lcd_line_four();
    lcd_write_string(PSTR("Code v1.4 / Tiasha"));
    //wait 5 minutes for next reading
    delay_ms(5000);
  }

  return 0;
}
```